Numerical analysis of a photonic crystal fiber based on two polarized modes for biosensing applications*

Qin Wei(秦 伟), Li Shu-Guang(李曙光)†, Xue Jian-Rong(薛建荣), Xin Xü-Jun(辛旭军), and Zhang Lei(张 磊)

Key Laboratory of Metastable Materials Science and Technology, College of Science, Yanshan University, Qinhuangdao 066004, *China*

(Received 21 December 2012; revised manuscript received 7 January 2013)

This paper presents a theoretical study on a photonic crystal fiber plasmonic refractive index biosensor. The proposed photonic crystal fiber sensor introduces the concept of simultaneous detection with the linearly polarized and radially polarized modes because the sensing performance of the sensor based on both modes is relatively high, which will be useful for selecting the modes to make the detection accurately. The sharp single resonant peaks of the linearly polarized mode and radially polarized mode, are stronger and more sensitive to the variation of analyte refractive index than that of any other polarized mode in this kind of photonic crystal fiber. For linearly polarized mode and radially polarized mode, the maximum sensitivities of 10448.5 nm per refractive index unit and 8230.7 nm per refractive index unit can be obtained, as well as 949.8 and 791.4 for figure of merits in the sensing range of 1.33–1.45, respectively. Compared with the conventional Au-metalized surface plasmon resonance sensors, our device is better and can be applied as a biosensor.

Keywords: photonic crystal fiber, sensors, surface plasmon

PACS: 42.81.−i, 42.81.Pa, 71.45.Gm **DOI:** 10.1088/1674-1056/22/7/074213

1. Introduction

The surface plasmon resonances (SPRs) have many potential applications, such as optical sensing,[1,2] optical filtering,[3] and near-field tips for sub-wavelength-scale imaging.[4,5] Recently, surface plasmon resonance sensors have attracted much attention especially the label-free fiber-optic biosensor. Biosensors have fascinated continuous research interests in detecting the analyte bulk refractive index changes, as well as monitoring formation of the nanometer-thin biolayers on top of the metallized sensor surface. For example, Hassani *et al.*[6] demonstrated an SPR biosensor, whose biolayer thickness resolution is as low as 0.039 nm in the whole 600 nm–920 nm region. Rindorf *et al.*[7] reported a sensitivity of 1.4-nm shift of a long-period grating resonance per nm thickness of the biolayer (1.4 nm/nm).

Photonic crystal fiber (PCF) with a regular hexagonal array of air holes running along the propagation direction can provide a flexible platform for sensing.[8–10] The combination of photonics technology and plasmonics science benefited from the development of coating technique and the SPR sensors based on the PCF have been widely investigated theoretically and experimentally in recent years.[11–16] Among these extensively investigated PCF-SPR refractive index sensors, most research was dedicated to multi-channel sensing.[11–14] In fact, the interference between neighboring channels is inevitable. The resonances between the fundamental core mode and the higher order plasmonic modes give rise to multiple resonance peaks, which lead to a worse detection limit. In a recent paper, Shuai *et al.*[15] presented and numerically characterized a closed-form multi-core holey fiber based on the plasmonic sensor with only one metalized analyte channel. However, they only utilized one mode of the multi-core holey fiber as other modes were weakly coupled with the higher surface plasmon polariton (SPP) modes and less sensitive to the refractive index change.

In this paper, we numerically characterize a plasmonic refractive index biosensor based on the single metalized analyte channel in PCF by using the finite element method (FEM). It is found that the novel biosensor demonstrates a sharp single resonance feature and high sensitivity. The resonant peaks, which come from not only the coupling between the linearly polarized HE_{11} mode and the first-order SPP mode, but also the coupling between the radially polarized mode TM_{01} and the fundamental SPP mode, play a key role in the coupling process. It is found that the fundamental SPP mode is coupled with the core-guide mode for the first time in the plasmonic sensing scheme, to the best of our knowledge. In Section 2, the structure design and theoretical modeling are given in detail, which will be followed by the discussion of simulation results. Then, the influence of the thickness of the gold layer and the central metalized analyte channel diameter are also studied which are helpful to the structure optimization. Furthermore, the biosensing applications of the proposed PCF-SPR biosensor are presented. The conclusions are given in the last section.

*Project supported by the National Natural Science Foundation of China (Grant Nos. 61178026 and 60978028), the Specialized Research Fund for the Doctoral Program of Higher Education of China (Grant No. 20091333110010), and the Natural Science Foundation of Hebei Province, China (Grant No. E2012203035).

†Corresponding author. E-mail: shuguangli@ysu.edu.cn

© 2013 Chinese Physical Society and IOP Publishing Ltd

2. Structure design and theoretical modeling

The schematic diagram of the PCF-SPR refractive index biosensor with a ring-shape core is shown in Fig. 1. This index-guiding PCF consists of two layers of air holes arranged in a regular hexagonal way, which can also generate hollow beams in the ring-shape region the same as that mentioned in Ref. [17]. Light will be transmitted in this ring-shape region, and it can only support the Gaussian beam. The hole-to-hole pitch Λ, the distance between the center air hole and the air hole of the first layer, is 2.0 μm. The diameters of the cladding air holes and central metalized analyte channel are $d = 0.4\Lambda$ and $d_c = \Lambda$, respectively. The thickness of the gold layer is $t = 40$ nm. Simply, the refractive index of the fiber material is assumed to be 1.45. The dielectric constant of gold is defined by the Drude-Lorentz model,[18] and the equation can be written as follows:

$$\varepsilon_m = \varepsilon_\infty - \frac{\omega_D^2}{\omega(\omega + j\gamma_D)} - \frac{\Delta\varepsilon\Omega_L^2}{(\omega^2 - \Omega_L^2) + j\Gamma_L\omega}, \quad (1)$$

where ε_m is the permittivity of gold, ε_∞ is the permittivity in the high frequency, $\Delta\varepsilon = 1.09$ is a weighting factor, ω is the angular frequency of the guided light, ω_D and Γ_D, $\omega_D/2\pi = 2113.6$ THz and $\Gamma_D/2\pi = 15.92$ THz, are the plasma frequency and damping frequency, respectively, Ω_L and Γ_L, $\Omega_L/2\pi = 650.07$ THz and $\Gamma_L/2\pi = 104.86$ THz, are the frequency and spectral width of the Lorentz oscillator. The FEM is used for investigating the mode characters and finding the complex propagation constants of the plasmonic and the core-guide modes. A perfectly matched layer (PML) with several micrometers is added to the outmost layer, which is used for absorbing the radiation energy. Moreover, a scattering boundary condition outside the PML region is used to reduce the reflections. In this paper, the coupled mode theory has been deployed to investigate the coupling between the surface plasmon and core-guided modes.[19] The intersection point of the dispersion curves for the plasmonic mode and core-guided mode, which corresponds to the largest energy transmission from the core-guided mode to the plasmonic mode, is used for locating the resonance wavelength.[11] The confinement loss can be obtained through

$$L = 8.686 \times \frac{2\pi}{\lambda} \mathrm{Im}(n_{\mathrm{eff}}) \times 10^4, \quad (2)$$

which is proportional to the imaginary part of the mode effective refractive index. The units of the confinement loss and the wavelength are dB/cm and micrometer, respectively.

With regard to fabrication, the proposed structure should be relatively easy to fabricate due to the gradually mature coating technique and the regular hexagonal array of air holes design. In a previous study, a selective coating technique for PCF had been successfully demonstrated experimentally.[20] We believe that our PCF-SPR biosensor can be successfully implemented with a precise fabricating process.

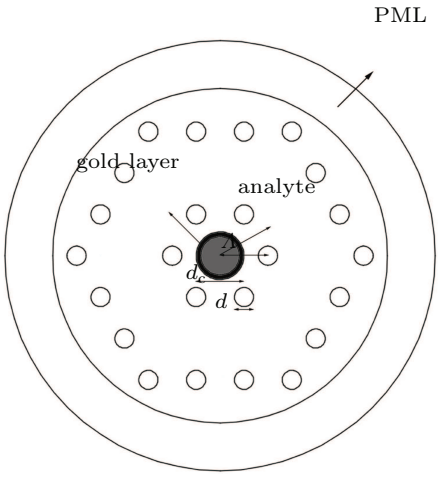


Fig. 1. Schematic diagram of the PCF-SPR refractive index biosensor with a ring-shape core. Cross section of the PCF-SPR sensor where the second layer of air holes has been removed to form the ring-shape core.

3. Numerical results

3.1. Mode analysis

We begin our analysis of the various core-guided modes in this kind of PCF to obtain a comprehensive understanding about the resonance properties. The structure parameters of the PCF are $d_c = \Lambda$, $d = 0.4\Lambda$, $t = 40$ nm, $n_a = 1.42$, and $\lambda = 700$ nm. By using the FEM solver to numerically simulate the designed PCF, the power flow distributions of the core-guided modes supported by this kind of PCF are illustrated in Fig. 2. Red arrows indicate the orientation of electric field in each mode. Besides the fundamental mode HE_{11} (Fig. 2(a)), the first higher order mode group in this fiber comprises the radially polarized mode TM_{01} (Fig. 2(b)) and azimuthally polarized mode TE_{01} (Fig. 2(c)). One mixed state HE_{21} (Fig. 2(d)) is also excited in the fiber. For HE_{11} mode and HE_{21} mode, there is another degenerate one with the same real part of effective refractive index but electric field orientation perpendicular to each other, respectively. All these modes excited in the fiber are able to resonate with plasmonic modes except for the TE_{01} mode within our computation accuracy. However, the HE_{21} mode is weakly coupling and less sensitive to the refractive index change, hence, we will concentrate on the coupling and sensing properties analysis of the HE_{11} and TM_{01} modes in the following study. In previous studies, there were many methods to achieve selection of the cylindrically polarized beam,[21,22] hence, the mode selection can be realized. Figures 3(a) and 3(b) illustrate the electric field distributions and the corresponding dispersion relations of the fundamental SPP and first-order SPP modes, respectively. The origin of these SPP modes can be explained by the ray model proposed in Ref. [4].

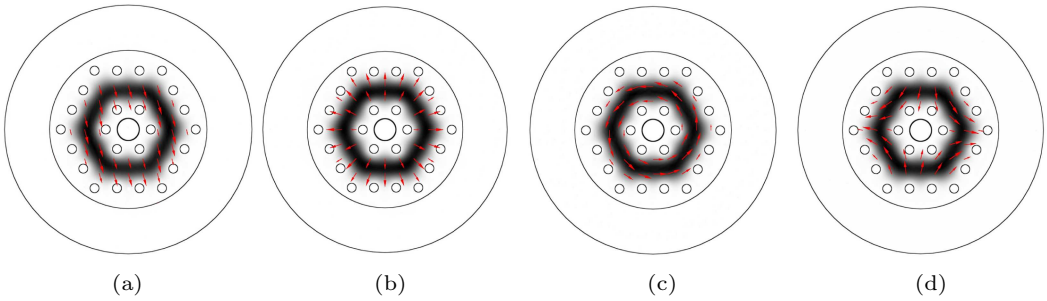


Fig. 2. (color online) Power flow distributions of core-guided modes in this kind of PCF. Red arrows represent the direction of electric field. Calculated for $d_c = \Lambda$, $d = 0.4\Lambda$, $t = 40$ nm, $n_a = 1.42$, and $\lambda = 700$ nm. (a) HE_{11} mode, (b) TM_{01} mode, (c) TE_{01} mode, and (d) HE_{21} mode.

3.2. Results and discussion

To investigate the coupling properties of the novel biosensor, the resonant curves for analyte refractive index $n_a = 1.42$ are depicted in Fig. 3. The phase-matching wavelength is the one at which the real part of effective refractive index of the core-guided mode and that of the plasmonic mode intersect. That means the largest energy transmission from the core-guided mode to the plasmonic mode as we can see from the loss spectra of the core-guided modes. Therefore, the intersections of the two lines (solid and dashed lines) in Figs. 3(a) and 3(b), present the corresponding resonant wavelengths 776 nm and 801 nm, respectively. From the inset (a3) or inset (b3) of Fig. 3, it is an obvious electric field overlapping, while the field is confined in the core and metal-analyte interface at a wavelength away from the resonant wavelength (insets (a1), (a2), (a4), (a5), and (b1), (b2), (b4), (b5) of Fig. 3). It is worth noting that the two modes loss spectra in Fig. 3 exhibit a sharp single-resonance feature, which is not influenced by the other higher order plasmonic modes.[15]

Next, we will discuss the characterization of sensitivity of the novel PCF-SPR biosensor. Typically, a refractive index sensor has a resonant feature whose resonant wavelength depends on the refractive index of the analyte. In this case, the sensitivity is defined as[23]

$$S_\lambda = \frac{\mathrm{d}\lambda_{\mathrm{peak}}(n_a)}{\mathrm{d}n_a}. \tag{3}$$

The resonant wavelengths λ_{peak} with respect to the analyte refractive indexes n_a of the two polarized modes are summarized in Table 1.

Table 1. Summary of n_a and λ_{peak} of the two modes.

	n_a	1.33	1.34	1.35	1.36	1.37	1.38	1.39	1.40	1.41	1.42	1.43	1.44	1.45
HE_{11}	λ_{peak}/nm	571	580	592	605	621	641	665	694	730	776	838	917	1019
TM_{01}	λ_{peak}/nm	574	585	597	612	630	652	678	711	752	801	860	927	1000

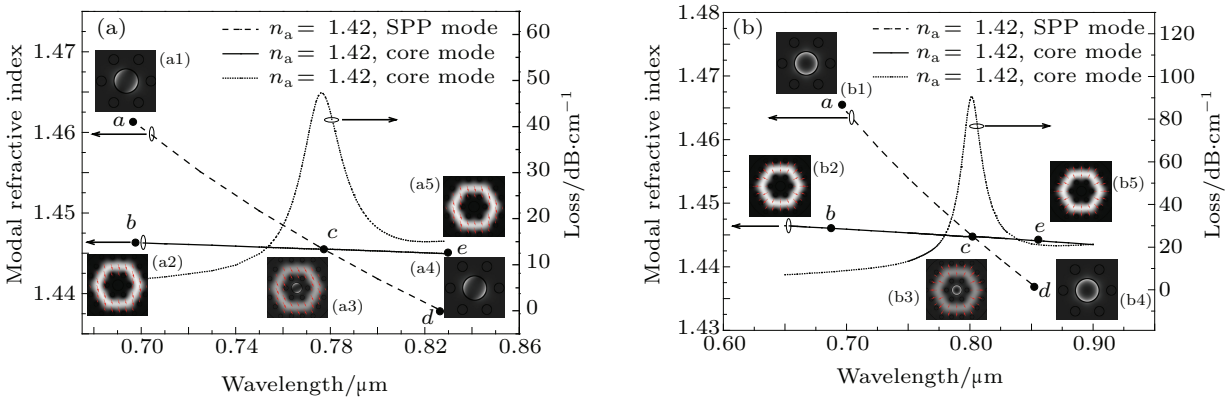


Fig. 3. (color online) (a) Calculated loss spectrum (dotted line) and dispersion relations of HE_{11} mode (solid line) and first-order SPP mode (dashed line). (b) Calculated loss spectrum (dotted line) and dispersion relations of TM_{01} mode (solid line) and fundamental SPP mode (dashed line). Insets (a1), (a2), (a3), (a4), (a5) and (b1), (b2), (b3), (b4), (b5) are electric field distributions of various modes.

In order to get the relation of sensitivity and analyte refractive index accurately, we introduce polynomial fitting to analyze these dates in Table 1. The fitting formula of the resonance wavelength versus the analyte refractive index for HE_{11} and TM_{01} modes are given by

$$\lambda_{\mathrm{peak}} = 323135.1981n_a^3 - 1311374.8751n_a^2 + 1775199.9417n_a - 800977.6274, \tag{4}$$

$$\lambda_{\mathrm{peak}} = 147435.8974n_a^3 - 584448.0519n_a^2 + 773214.3024n_a - 340833.4885. \tag{5}$$

According to Eqs. (3), (4), and (5), we can get the relational expression of sensitivity versus analyte refractive index, and

the curves of sensitivity for the HE_{11} and TM_{01} modes are depicted in Fig. 4(a). Generally speaking, the performance of any SPR sensor is evaluated in terms of three key aspects. Signal to noise ratio (SNR) and spectral width are another two typical features besides the sensitivity, which can both contribute to a better detection limit. This can also be demonstrated using the more widely accepted figure of merit[24]

$$\mathrm{FOM} = \frac{\mathrm{m(eV \cdot RIU^{-1})}}{\mathrm{FWHM(eV)}}, \tag{6}$$

where m is the slope of the resonance peak position per refractive index unit (RIU) and FWHM is the full width at half-maximum in eV. Considering both the absolute shift in energy and the width of the resonance peak, it indicates the sensitivity of the system better. A higher figure of merit (FOM) means a better detection limit. Figure 4(b) depicts the FOM with the change of the analyte index.

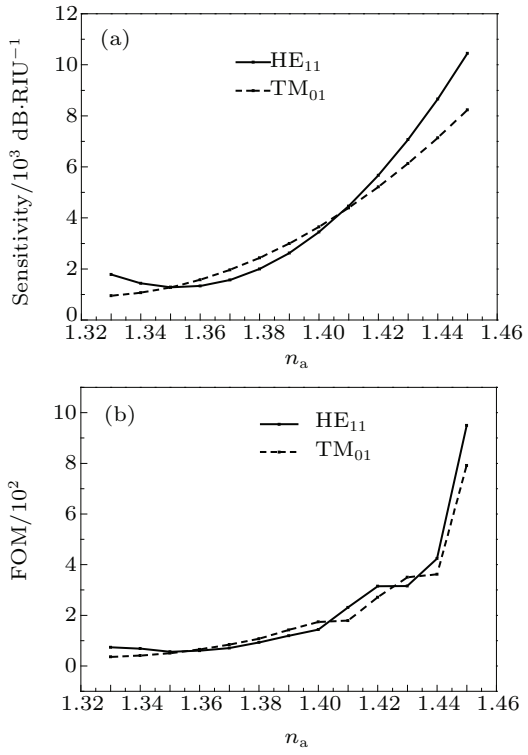


Fig. 4. (a) Sensor sensitivity and (b) FOM with the change of analyte index for HE_{11} (solid line) mode and TM_{01} (dashed line) mode, respectively.

From Fig. 4, we know that the sensor sensitivity is higher if the analyte refractive index is larger, so the sensor with high refractive index analyte will be a better one. It is clear that the sensitivity of the sensor based on HE_{11} mode is larger than that of the one based on TM_{01} mode outside the range of 1.35–1.408, so we can select the higher sensitive modes in different refractive index ranges and finally propose the PCF-SPR biosensor for high accuracy measurement. The average sensitivities of other sensors, such as the holey fiber with a small air hole in the core,[11] holey fiber with an analyte-filled core,[12] multi-core holey fiber,[15] polished multimode fiber,[25] and tilted grating in SMF,[26] are about 2728 nm/RIU in the sensing range from 1.33 to 1.41, 2775 nm/RIU from 1.33 to 1.42, 2929.39 nm/RIU from 1.33 to 1.42, 956 nm/RIU from 1.328 to 1.345, 454 nm/RIU from 1.4211 to 1.4499, respectively. The maximum sensitivities of our proposed one are 10448.5 nm/RIU for HE_{11} mode and 8230.7 nm/RIU for TM_{01} mode, which are higher than those of the mentioned sensors above. In addition, FOMs of two modes in our proposed fiber can reach 949.8 and 791.4 when n_a is 1.45, which are higher than the values 73 in Ref. [11] and 216 in Ref. [27].

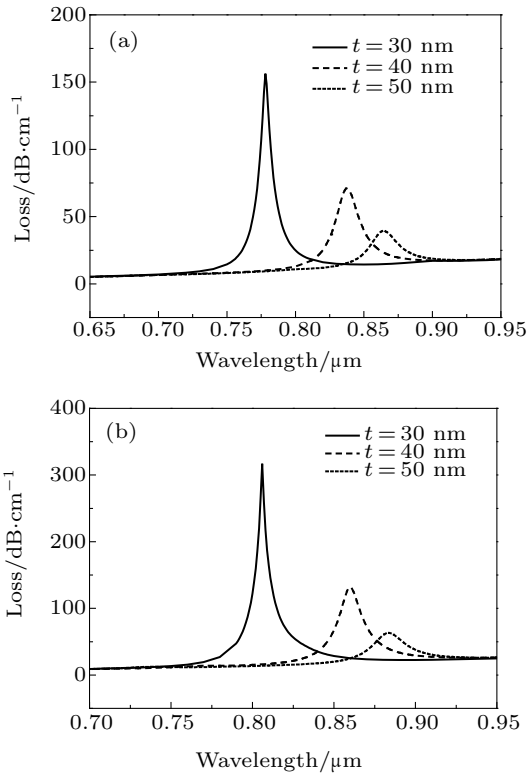


Fig. 5. (a) and (b) Loss spectra of the single resonant peak for thickness of a gold coating of 30 nm, 40 nm, and 50 nm for HE_{11} and TM_{01} modes, respectively.

In what follows, we will study the influence of the thickness of the gold layer and the central metalized analyte channel diameter d_c for the plasmon excitation in the novel PCF. Surface plasmon waves are very sensitive to the thickness of metallic layers. As illustrated in Fig. 5, the loss spectra vary considerably with the gold layer thickness changing from 30 nm to 50 nm when n_a is 1.43. The resonant peak position shifts to a longer wavelength as the gold layer increases, however, the modal propagation loss at resonance decreases and FWHM is broadened when the gold layer becomes thicker. This sensitivity of the resonant wavelength to the gold thickness can be used in the study of metal nanoparticle binding events on the metallic surface of the biosensor.[28] In this particular design, we can tune the central metalized analyte channel diameter d_c to optimize the structure of the PCF-SPR biosensor. The simulated results are presented in Fig. 6. For a

constant $d = 0.4\Lambda$, with the increase of d_c, the sensitivity increases whilst the resonant spectra becomes deeper, which will keep a better SNR. For example, the separations of the resonant wavelengths of HE_{11} mode between two analyte refractive indexes n_a = 1.43 and n_a = 1.44 are 68 nm for $d_c = 0.9\Lambda$, 79 nm for $d_c = 1.0\Lambda$, and 92 nm for $d_c = 1.1\Lambda$. Similarly, those of the TM_{01} mode between two analyte refractive indexes n_a = 1.43 and n_a = 1.44 are 56 nm for $d_c = 0.9\Lambda$, 67 nm for $d_c = 1.0\Lambda$, and 78 nm for $d_c = 1.1\Lambda$, respectively. The design parameters in this work are optimized ones to some extent.

It has been demonstrated that the PCF structure makes it possible to design a biosensor with different sensitivities with respect to the two modes (HE_{11} and TM_{01}). Certainly, the future development of the proposed structure also depends on the proper design of the air hole diameters d. We believe that the sensing performance and detection limit can be better and further work is ongoing.

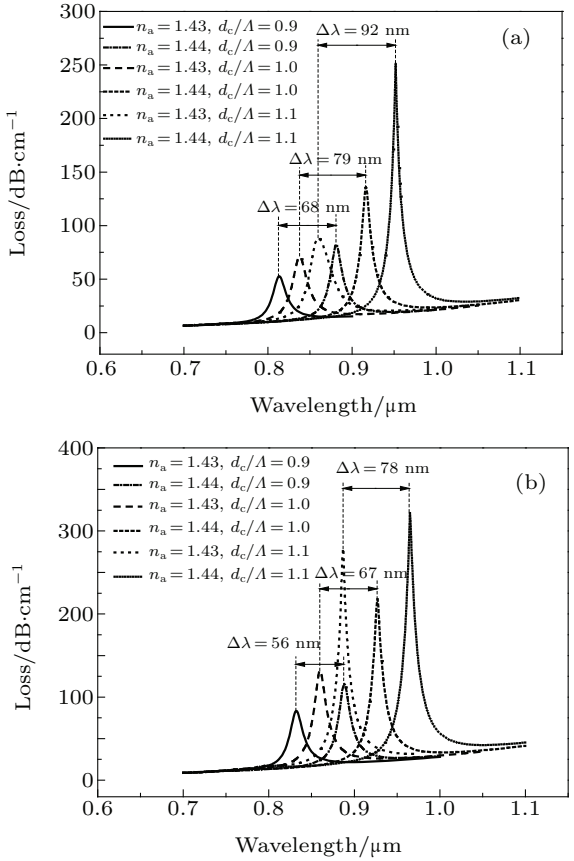


Fig. 6. (a) and (b) Loss spectra of the single resonant peak for the central metalized analyte channel diameter of 0.9Λ, 1.0Λ, and 1.1Λ for HE_{11} and TM_{01} modes, respectively.

4. Applications

SPR biosensors have found extensive applications in the detection of chemical and biological compounds in areas such as medical diagnostics, food safety control, environmental protection, and drug detection.[29] In this paper, it has been shown that gold-coated PCF can be used for sensing analysis of biomolecules, such as proteins[7] and water.[30] Generally, the detection and identification of biological and chemical analytes are obtained by measuring resonant wavelength or finding the peak of the transmission loss spectrum corresponding to the resonant wavelength of the PCF-SPR biosensor. Infiltration techniques have been previously demonstrated both theoretically and experimentally,[7,11,30] where the aqueous samples were introduced into the PCF either by utilizing capillary forces or by applying pressure. Thus we consider that it is possible to introduce the analytes refractive index range from 1.33 to 1.45 into the hole of our proposed fiber.

Experimental measurements with the PCF biosensor have shown that a refractive index of $n_a = 1.45$ for α-streptavidin biomolecules is a realistic assumption.[7] A selective filling technique of the central air hole of a PCF was demonstrated in Ref. [30]. The approach described involves the use of a UV curable adhesive, and the filling of the central hole alone is achieved in three steps. Step (i) Injecting the UV curable polymer into the holes of the PCF by a syringe pump. After a period of time, the infiltration length of the larger hole in the center of the PCF is longer than that of the other small holes of the PCF. This phenomenon can be explained by the equation $v = -\Delta p r^2/8l\mu$, where v represents the average velocity of the liquid flow in the air hole, r is the radius of the hole, Δp can be interpreted as the pressure difference between the two ends of the liquid tube within the cylindrical hole, l is the infiltration length of the liquid within the hole, and μ is the viscosity of the liquid. Subsequently, the fiber is cleaved at a suitable position to ensure that only the central hole is capped by the cured polymer. Step (ii) Filling the fiber with UV curable polymer again, which, since the central hole of the PCF is now blocked, will result in only the small holes being filled. The UV curable polymers in the small holes need to be penetrated beyond the length of the cap in the central hole by applying pressure on the syringe pump. Then, we cut the fiber once again to ensure that the small holes are blocked by the cured polymer but the central hole is open. Step (iii) Injecting the α-streptavidin solution into the central hole by using the syringe pump. Finally, the fiber is cleaved to cause a hybrid PCF with the central hole filled with the desired analytes solution while the fiber cladding consists of an array of air holes. If the analyte solution has been fixed, the resonant wavelength can be obtained from Eq. (4) or Eq. (5). Conversely, by measuring the peak of the transmission loss spectrum corresponding to the resonant wavelength of the PCF-SPR biosensor, the introduced unknown analytes can be labeled. The technique may thus be used for label-free detection of biomolecules and chemical compounds in the refractive index ranges from 1.33–1.45 by using our high sensitivity PCF-SPR biosensor. From a biochemical point of view, the label-free detection of biomolecules is greatly appealing, since it opens up new possibilities for photonic crystal fibers

to be used in surface chemistry studies, such as in drug discovery, sensors in point-of-care devices, and other laboratory equipment.

5. Conclusions

Numerical characteristics of a PCF-SPR biosensor have been presented in this paper. The only larger metalized analyte channel will not only reduce the gold consumption, but also be free from the interference between neighboring metalized analyte channels. The possibility of using the two modes (HE_{11} and TM_{01}) to form a single resonance and highly sensitive biosensor has also been demonstrated. Simulation results confirmed that the sensing performance of the proposed PCF-SPR biosensor based on both modes (HE_{11} and TM_{01}) were relatively high, which could be useful for selecting the modes to make the detection accurately. In conclusion, it shows that this new PCF-SPR biosensor will be very useful for further studies in biochemical sensing applications and other fiber-based plasmonic devices.

References

[1] Lin K Q, Wei L M, Zhang D G, Zheng R S, Wang P, Lu Y H and Ming H 2007 *Chin. Phys. Lett.* **24** 3081
[2] Yang X Y, Liu D M, Xie W C and Li C F 2007 *Chin. Phys. Lett.* **24** 458
[3] Du Y, Li S G and Liu S 2012 *Chin. Phys. B* **21** 094219
[4] Schmidt M A, Prill Sempere L N, Tyagi H K, Poulton C G and Russell P S J 2008 *Phys. Rev. B* **77** 033417
[5] Lee H W, Schmidt M A, Tyagi H K, Prill Sempere L and Russell P S J 2008 *Appl. Phys. Lett.* **93** 111102
[6] Hassani A and Skorobogatiy M 2009 *J. Opt. Soc. Am. B* **26** 1550
[7] Rindorf L, Jensen J B, Dufva M, Pedersen L H, Høiby P E and Bang O 2006 *Opt. Express.* **14** 8224
[8] Yan F P, Wang L, Mao X Q, Gong T R, Liu P, Tao P L and Peng W J 2010 *Opt. Commun.* **283** 3658
[9] Yan F P, Li Y F, Wang L, Gong T R, Liu P, Liu Y, Tao P L, Qu M X and Jian S S 2008 *Acta Phys. Sin.* **57** 5735 (in chinese)
[10] Zhang L, Li S G, Yao Y Y, Fu B, Zhang M Y and Zheng Y 2010 *Acta Phys. Sin.* **59** 1101 (in chinese)
[11] Yu X, Zhang Y, Pan S S, Shum P, Yan M, Leviatan Y and Li C M 2009 *J. Opt.* **12** 015005
[12] Zhang Y T, Xia L, Zhou C, Yu X, Liu H R, Liu D M and Zhang Y 2011 *Opt. Commun.* **284** 4161
[13] Zheng L, Zhang X, Ren X M, Gao J, Shi L, Liu X L, Wang Q and Huang Y Q 2011 *Opt. Laser Technol.* **43** 960
[14] Hautakorpi M, Mattinen M and Ludvigsen H 2008 *Opt. Express.* **16** 8427
[15] Shuai B B, Xia L, Zhang Y T and Liu D M 2012 *Opt. Express.* **20** 5974
[16] Bing P B, Li Z Y, Yao J Q, Lu Y, Di Z G and Yan X 2012 *Optoelectron. Lett.* **8** 245
[17] Zhang X X, Li S G, Liu S, Du Y and Zhu X P 2012 *Opt. Commun.* **285** 5079
[18] Vial A, Grimault A S, Macías, Barchiesi D and de la Chapelle M L 2005 *Phys. Rev. B* **71** 085416
[19] Ditlbacher H, Galler N, Koller D M, Hohenau A, Leitner A, Aussenegg F R and Krenn J R 2008 *Opt. Express.* **16** 10455
[20] Zhang X, Wang R, Cox F M, Kuhlmey B T and Large M C J 2007 *Opt. Express.* **15** 16270
[21] Jocher C, Jauregui C, Voigtländer C, Stutzki F, Nolte S, Limpert J and Tünnermann A 2011 *Opt. Express.* **19** 19582
[22] Moreno I, Davis J A, Ruiz I and Cottrell D M 2010 *Opt. Express.* **18** 7173
[23] Gauvreau B, Hassani A, Fehri M F, Kabashin A and Skorobogatiy M 2007 *Opt. Express* **151** 11413
[24] Sherry L J, Chang S H, Schatz G C, Duyne R P V, Wiley B J and Xia Y N 2005 *Nano Lett.* **5** 2034
[25] Peng W, Banerji S, Kim Y C and Booksh K S 2005 *Opt. Lett.* **30** 2988
[26] Shevchenko Y Y and Albert J 2007 *Opt. Lett.* **32** 211
[27] Tian M, Lu P, Chen L, Lv C and Liu D M 2012 *Opt. Commun.* **285** 1550
[28] Hassani A, Gauvreau B, Fehri M F, Kabashin A and Skorobogatiy M 2008 *Electromagnetics* **28** 198
[29] Lee B, Roh S and Park J 2009 *Opt. Fiber Technol.* **15** 209
[30] Huang Y Y, Xu Y and Yariv A 2004 *Appl. Phys. Lett.* **85** 5182